Exploratory ASCA Observations of Broad Absorption Line Quasi-Stellar Objects

S. C. Gallagher, W. N. Brandt and R. M. Sambruna
Department of Astronomy and Astrophysics, Penn State University, 525 Davey Lab, University Park, PA 16802

S. Mathur
Harvard-Smithsonian Center for Astrophysics, 60 Garden Street, Cambridge, MA 02138

N. Yamasaki
Department of Physics, Faculty of Science, Tokyo Metropolitan University, 1-1 Minami-Osawa, Hachioji, Tokyo 192-03, Japan

ABSTRACT

We present the analysis and interpretation of a sample of eight *ASCA* observations of Broad Absorption Line Quasi-Stellar Objects (BALQSOs). This is the first moderate-sized sample of sensitive BALQSO observations above 2 keV, and the BALQSOs in our sample are among the optically brightest known ($B = 14.5$–18.5). Despite the ability of 2–10 keV X-rays to penetrate large column densities, we find BALQSOs to be extremely weak sources above 2 keV, and we are only able to add two new 2–10 keV detections (0226–104 and IRAS 07598+6508) to those previously reported. By comparison with non-BALQSOs of similar optical continuum magnitudes, we derive the column densities needed to suppress the expected X-ray fluxes of our BALQSOs. In several cases we derive column densities $\gtrsim 5 \times 10^{23}$ cm^{-2} for a neutral absorber with solar abundances. These are the largest X-ray column densities yet inferred for BALQSOs, and they exceed *ROSAT* lower limits by about an order of magnitude.

Optical brightness does not appear to be a good predictor of 2–10 keV brightness for BALQSOs, but our data do suggest that the BALQSOs with high optical continuum polarizations *may* be the X-ray brighter members of the class. For example, the highly polarized object PHL 5200 appears to be unusually X-ray bright for a BALQSO given its optical magnitude.

We discuss the implications of our results for future observations with *AXAF* and *XMM*. If the objects in our sample are representative of the BALQSO population, precision X-ray spectroscopy of most BALQSOs will unfortunately prove difficult in the near future.

Subject headings: galaxies: active – QSOs: absorption lines – X-rays: galaxies

1. Introduction

While Broad Absorption Line Quasi-Stellar Objects (BALQSOs) allow us to view substantial and energetically important gas outflows that are probably present in most QSOs (e.g. Weymann 1997), their study in the X-ray regime has not yet matured. BALQSOs are known to be much weaker in the soft X-ray band (< 2 keV) than QSOs that lack BALs (e.g. Kopko et al. 1994; Green et al. 1995; Green & Mathur 1996, hereafter GM96), and only a few BALQSOs have reliable X-ray detections. Their low soft-X-ray fluxes may arise as a result of photoelectric X-ray absorption by the same outflowing matter that makes the BALs in the ultraviolet. Hard X-ray (> 2 keV) observations of BALQSOs can in principle test the absorption hypothesis as well as constrain the properties, in particular the column densities, of BALQSO outflows. Column density constraints for BALQSOs are difficult to obtain from ultraviolet data due to BAL saturation (e.g. Arav 1997; Hamann 1998), and the limited X-ray data now available suggest that previous column density estimates from ultraviolet lines were too small by a factor of ≈ 100 or more. Because the photoelectric X-ray absorption cross section is a strongly decreasing function of energy, BALQSOs that are weak in the soft X-ray band (e.g. for *ROSAT*) could be much brighter at higher X-ray energies (e.g. for *ASCA*).[1] In the hard X-ray band, only the BALQSOs PHL 5200 ($z = 1.98$, $B \approx 18.5$) and Mrk 231 ($z = 0.042$, $B \approx 14.5$) have been studied in detail. Mathur, Elvis & Singh (1995) argue for the presence of heavy X-ray absorption with $N_{\rm H} \sim 1 \times 10^{23}$ cm^{-2} in PHL 5200, although the observed flux is low making reliable spectral analysis difficult (see §3 for further discussion). The *ASCA* data for Mrk 231 also suggest a large intrinsic column density ($\sim 2 \times 10^{22}$–10^{23} cm^{-2}; Iwasawa 1999; Turner 1999).

Since at least $\approx 10\%$ and perhaps up to 30–50% of all QSOs have BAL gas along our line of sight (e.g. Goodrich 1997; Krolik & Voit 1998), our lack of knowledge about the X-ray properties of BALQSOs represents a serious deficiency. In an attempt to remedy this situation, we performed *ASCA* observations of several of the BALQSOs that seemed most likely to be X-ray bright above 2 keV. Given the unknown hard X-ray properties

---

[1]The *ROSAT* band is from 0.1–2.4 keV and peaks from 0.9–1.4 keV, while the *ASCA* band is from 0.6–9.5 keV and has high sensitivity in the 3–7 keV range. To good approximation, the photoelectric X-ray absorption cross section is proportional to $E^{-\frac{8}{3}}$. Thus a 6 keV X-ray is ≈ 120 times more penetrating than a 1 keV X-ray.

(e.g. fluxes) of BALQSOs, we adopted a conservative strategy of making moderate-depth 'exploratory' observations of a fairly large number of objects. In this manner, we could learn about the 2–10 keV properties of as many BALQSOs as possible without being too heavily invested in the uncertain results from any one object. BALQSOs found to be reasonably X-ray bright based on exploratory observations could then be followed up with deeper X-ray spectroscopic observations. We chose as our targets some of the optically brightest (in the B and R bands) BALQSOs, since there is a general correlation between optical brightness and intrinsic X-ray brightness for QSOs (e.g. Zamorani et al. 1981). In this paper we present *ASCA* results for five of the optically brightest BALQSOs known: PG 0043+039, 0043+008, 0226–104, PG 1700+518 and LBQS 2111–4335. In the B band, these objects are all brighter than the *ASCA*-detected BALQSO PHL 5200. In addition, we include the *ASCA* results from archived observations of IRAS 07598+6508, Mrk 231 and PHL 5200. Redshifts, B and R magnitudes, and Galactic column densities for the BALQSOs in our sample are given in Table 1. Many of our BALQSOs are comparably bright in the optical band to radio-quiet (RQ) QSOs which *ASCA* has studied in significant detail (e.g. PG 1634+706 and PG 1718+481, Nandra et al. 1995; IRAS 13349+2438, Brandt et al. 1997), and our sample is on average significantly brighter at B than the high-redshift RQ QSOs studied with *ASCA* by Vignali et al. (1999). Aside from being some of the optically brightest BALQSOs in the sky, the objects in our sample span a range of other properties (e.g. absorption line strength, absorption line shape, redshift, optical continuum polarization, infrared luminosity). While they do not form a rigorously defined complete sample, they do appear to comprise a reasonably representative subsample of the BALQSO population as a whole.

As mentioned above, if BALQSOs suffer from heavy X-ray absorption then they will be much brighter above 2 keV than at lower energies. For example, a hypothetical BALQSO at $z = 2$ with an absorption column density of 5×10^{23} cm^{-2} is expected to be ≈ 20 times brighter in the 2–10 keV band than in the 0.1–2.0 keV band (observed-frame with a photon index of $\Gamma = 2.0$ for the underlying power law). The 2–10 keV sensitivity of *ASCA* thus makes it a superior tool to *ROSAT* for studying BALQSOs with X-ray column densities in the wide range from $\approx (1\text{–}500)\times 10^{22}$ cm^{-2} (column densities substantially larger than $\sigma_{\rm T}^{-1} = 1.50 \times 10^{24}$ cm^{-2} are optically thick to Thomson scattering and are thus impenetrable to X-rays with energies below $m_{\rm e}c^2$). Furthermore, even moderate-length *ASCA* non-detections can set important constraints on the 2–10 keV fluxes and internal column densities of BALQSOs. These are important for planning *AXAF*/*XMM* spectroscopic observations, and in some cases *ASCA* non-detections can raise the current *ROSAT* lower limits on BALQSO X-ray column densities by roughly an order of magnitude (from $\approx 5 \times 10^{22}$ cm^{-2} to $\approx 5 \times 10^{23}$ cm^{-2}). If the outflowing BAL material causes the inferred X-ray absorption, this increases the implied BALQSO mass outflow rates and kinetic luminosities.

2. Observations and Data Analysis

2.1. Observation Details and Data Reduction

In Table 1 we list the relevant observation dates, exposure times and instrument modes for our objects. The data resulting from these observations were reduced and analyzed with FTOOLS and XSELECT following the general procedures described in Brandt et al. (1997). We have used Revision 2 data (Pier 1997) and adopted the standard Revision 2 screening criteria.

2.2. Image Analyses and Count Rate Constraints

We used XSELECT to create full (0.6–9.5 keV for SIS and 0.9–9.5 keV for GIS) and hard (2–9.5 keV) band images for each of the four *ASCA* detectors. We also created summed SIS0+SIS1 and GIS2+GIS3 images in the full and hard bands. Image analysis was performed using XIMAGE (Giommi, Angelini & White 1997). We first attempted to independently check the *ASCA* astrometry using serendipitous X-ray sources within the fields of view. We correlated *ASCA* serendipitous source positions with objects in coincident *ROSAT*/*Einstein* images as well as the NED/SIMBAD databases. We were able to independently verify the astrometry for the observations of all BALQSOs but PG 0043+039, Mrk 231 and PHL 5200. We comment that the *ASCA* astrometry is generally quite reliable (see Gotthelf 1996), and our independent checking is only done for confirmation.

We then searched all the images described above for any significant X-ray sources that were positionally coincident with the precise optical positions of our BALQSOs. In order to determine the observed SIS count rate or upper limit for a given BALQSO, the 0.6–9.5 keV counts were extracted from a circular target region with a $3.2'$ radius centered on the optical BALQSO position. This provided counts for the target region, $N_{\rm t}$. An annular or circular source-free background region was chosen and similarly extracted to give background counts. The background counts were normalized to the area of the target region to obtain $N_{\rm b}$ which was then subtracted from $N_{\rm t}$. If the difference was $< 3\sigma$ where $\sigma = \sqrt{N_{\rm b}}$, the observation was considered a non-detection. In this case an upper limit on the count rate was taken to be $3\sqrt{N_{\rm t}}/t_{\rm e}$ where $t_{\rm e}$ is the exposure time listed in Table 1. For observations with $\geq 3\sigma$ detections, the count rate was calculated as $(N_{\rm t} - N_{\rm b})/t_{\rm e}$. A similar procedure was followed for the GIS detectors. However, for the GIS the extracted energy range was from 0.9–9.5 keV, and the radius of the target region was $5'$. The results of these analyses are presented in Table 2, and we comment on special cases in §3. Only four of these optically bright BALQSOs were detected with high statistical significance: 0226–104, IRAS 07598+6508, Mrk 231 and PHL 5200. We have chosen our target region sizes based upon §7.4 of *The ASCA Data Reduction Guide*, and we have found that varying the target region sizes within the recommended ranges does not materially change our basic results. When calculating $N_{\rm b}$ we have investigated at least two background regions for each SIS/GIS image, and we find that our results also do not materially depend upon our choice of background region. When our SIS observations were made using 2 CCD mode (see Table 1), we took all background photons from the chip that contained the target.

We also give observed frame 2–10 keV fluxes or upper limits for our BALQSOs in Table 2. These were computed for SIS0 with PIMMS (Mukai 1997) using a power law with $\Gamma = 2$. The intrinsic column density was taken to be 1×10^{23} cm^{-2} or the value from column three of Table 3 (whichever is larger).[2] Note that cosmological redshifting of the X-ray spectrum can in some cases greatly reduce the effect of the intrinsic absorption. This allows us to set more sensitive upper limits on the 2–10 keV fluxes for some high redshift objects due to the energy dependence of the *ASCA* spectral response.

2.3. Column Density Constraints

Since X-ray spectra cannot be modeled for most of the BALQSOs in our sample, we have followed the method adopted by GM96 to place lower limits on their intrinsic column densities. Briefly, we assumed the underlying optical-to-X-ray continuum shape of a typical RQ QSO and added an intrinsic absorbing column until the predicted count rate matched our observed count rate or upper limit. This type of analysis relies upon the plausible but unproven assumption that our targets have typical RQ QSO X-ray continua viewed through an intrinsic absorbing column of gas. Comparisons of BALQSO and non-BALQSO optical/ultraviolet emission lines and continua show that these two types of QSOs are remarkably similar, consistent with the view that these are not two inherently different classes of objects (e.g. Weymann et al. 1991). We also take the gas in the absorbing column to have solar abundances (Anders & Grevesse 1989), and this appears to be consistent with

[2]In practice, PIMMS is only able to work with column densities at $z = 0$. Therefore, to include intrinsic column densities at $z > 0$ in PIMMS we used XSPEC (Arnaud 1996) to find the column density at $z = 0$ that produces equivalent absorption. Galactic absorption was also taken into account in this process.

the currently available data (see Arav 1997 and Hamann 1998). Further justification for the assumptions that underlie this general method may be found in GM96. One additional issue not discussed by GM96 is that resonant absorption lines may be a significant source of X-ray opacity due to the large velocity dispersions of BALQSO outflows (compare with §3 of Kriss et al. 1996). We have neglected this effect for consistency with all previous work and because there is presently no proof that the BAL gas also causes the inferred X-ray absorption. A detailed treatment of resonant absorption line opacity in the X-ray band will be complex and dependent upon the details of the velocity dispersion in the BAL outflow, but this opacity is expected to modify the inferred column density by less than a factor of ≈ 2 (J. Krolik, private communication). Theoretical calculations examining the importance of this effect would be a valuable addition to the literature.

The optical-to-X-ray spectral index, $\alpha_{\rm ox}$, is the slope of a nominal power law connecting the rest-frame flux density at 2500 Å to that at 2 keV (QSOs with large values of $\alpha_{\rm ox}$ are those that are X-ray faint). Typical RQ QSOs are observed to have $\alpha_{\rm ox} = 1.51 \pm 0.10$ (this value is from §4.3 of Laor et al. 1997 for an optical flux density at 2500 Å; A. Laor, private communication). The 2 keV flux density can be predicted given the rest-frame 2500 Å flux density and an expected value for $\alpha_{\rm ox}$. Flux densities at 2500 Å for PG 0043+039 and PG 1700+518 were obtained by interpolating the continuum flux density data of Neugebauer et al. (1987) with a power law. For our non-PG BALQSOs, we derived the flux density at 2500 Å from the observed B magnitude (see Table 1) using the flux zero point of Marshall et al. (1983) and extrapolating along an assumed optical continuum power law with slope $\alpha_{\rm o} = 0.5$. The Galactic extinction corrections used by GM96 and a K-correction for the power law were also included.

An $\alpha_{\rm ox}$ value of 1.6 was used to predict an underlying rest-frame flux density at 2 keV for each BALQSO in our sample. We chose this value of $\alpha_{\rm ox}$ for consistency with GM96 and note that it is reasonably conservative (also see the discussion in §4.1 of GM96). We assumed that the underlying X-ray continuum shape was a power law with photon index Γ, and we then calculated the expected power-law normalization at 1 keV in the observed frame. We entered this model into XSPEC (Arnaud 1996) allowing for the presence of absorption by a column of neutral gas intrinsic to the BALQSO. Galactic absorption was also included with the column densities given in Table 1. Using the simulation routine FAKEIT with the spectral response matrices for the *ASCA* SIS0 and GIS3 detectors [described in §10.4.1 of the AO-7 *ASCA* Technical Description (AN 98-OSS-03)], a predicted count rate was generated. The intrinsic column density was then increased until the predicted count rate from the simulation no longer exceeded the measured count rate or upper limit. In this manner, an *upper* limit on the count rate yielded a *lower* limit on the intrinsic column density. We have focused on the SIS0 and GIS3 detectors because for the standard pointing position our targets lie closer to the optical axes of these detectors. Combining like detectors (SIS0/SIS1 or GIS2/GIS3) would not substantially improve the column density constraints due to the fact that the vignetting for *ASCA* is highly dependent upon off-axis angle and is thus noticeably worse for SIS1 and GIS2. The results from this analysis are presented in Table 3. Since X-ray spectral shapes vary among the RQ QSO population, we have performed these calculations with both $\Gamma = 1.7$ and $\Gamma = 2.0$ in order to cover the typical range of photon index values (see Reeves et al. 1997). Using PG 0043+039 as an example, we have also illustrated the dependence of the inferred column density upon the intrinsic $\alpha_{\rm ox}$ value in Figure 1.

Recent evidence indicates that some, if not all, BALQSOs have significantly attenuated optical/ultraviolet continua compared to non-BAL RQ QSOs (e.g. Goodrich 1997; see this paper for the precise definition of 'attenuation'). In this case, an underlying flux density at 2 keV that is predicted from the attenuated flux density at 2500 Å will be artificially low. While this issue is difficult to address with precision at present, correcting for it would tend to strengthen our above results. Even larger intrinsic column densities would be required to suppress the larger predicted X-ray fluxes. For two of our BALQSOs with near-infrared continuum flux densities in the literature, PG 0043+039 and PG 1700+518, we have examined this matter by attempting to predict the underlying 2 keV flux density from the 1.69 μm flux density (again using the data of Neugebauer et al. 1987). Laor et al. (1994) argue that the 1.69 μm flux density is a reasonably good predictor of the 0.3 keV flux density, and the Laor et al. (1997) data show that it is also a reasonably good predictor of the 2 keV flux density. We have computed $\alpha_{\rm ix}$, the spectral slope of a nominal power law between 1.69 μm and 2 keV, for the 20 QSOs from Laor et al. (1997) without intrinsic absorption. We find that $\alpha_{\rm ix} = 1.29 \pm 0.09$, and that $\alpha_{\rm ix}$ has a comparable dispersion to $\alpha_{\rm ox}$ for the same set of QSOs. We have repeated our column density estimates for PG 0043+039 and PG 1700+518 using $\alpha_{\rm ix}$ in place of $\alpha_{\rm ox}$, and we find that the inferred column density lower limits are within a factor of two of those presented in Table 3. We show our results for PG 0043+039 in Figure 2, and for PG 1700+518 we find an intrinsic column density $> 8.5 \times 10^{23}$ cm^{-2} when $\alpha_{\rm ix} = 1.29$ and $\Gamma = 2.0$.

3. Notes on Individual Observations

PG 0043+039: The optical and ultraviolet properties of this BALQSO were recently studied in detail by Turnshek et al. (1994), and the *ASCA* analysis for it was straightforward. Our large inferred X-ray column density combined with the intrinsic color excess of $E(B-V) \approx 0.11$ may suggest that the absorber is dust poor (compare with §3.1.1

of Turnshek et al. 1994).

0043+008 (UM 275): Zamorani et al. (1981) claimed that this BALQSO was detected in a 1.6 ks *Einstein* observation, although our analysis of the *Einstein* data made us skeptical of this claim. Wilkes et al. (1994) also give only an *Einstein* upper limit. 0043+008 is undetected in our much deeper (23 ks) *ASCA* observation. Based on our analysis, it appears that the claimed *Einstein* detection was actually an unrelated source lying $2.1'$ from the precise optical position. In order to obtain the tightest possible constraints on the SIS and GIS count rates for 0043+008, we have excluded this source from the target regions before calculating the count rate upper limits. This source does not cause serious confusion, but there was a statistical photon excess in the target region for GIS3 that was not consistent with a point source or the optical position of 0043+008. We suspect this excess is due to imperfect removal of all the photons from the *Einstein* source.

0226–104: Despite the fact that this BALQSO has been intensively studied (e.g. Korista et al. 1992), the coordinates stated for it in the literature are inconsistent with each other. We have used the coordinates $\alpha_{2000} = 02^{\rm h}28^{\rm m}39^{\rm s}.2$, $\delta_{2000} = -10^\circ 11' 10.0''$ (T. Barlow, private communication). 0226–104 was detected in all but the SIS1 detector as a point source (the SIS1 non-detection can be understood as due to the larger off-axis angle of 0226–104 in this detector). We excluded counts from two nearby sources before calculating the count rates.

IRAS 07598+6508: This BALQSO was marginally detected by *ROSAT* with a count rate of $\approx 1.8 \times 10^{-3}$ count s^{-1}, but it was impossible to determine whether the observed X-ray emission was associated with accretion activity or a circumnuclear starburst (Lawrence et al. 1997). There was an X-ray source coincident with the optical position of IRAS 07598+6508 in the GIS3 detector, and the target region counts were 8.6σ above background for the full band image (the source was also seen in the hard band image). There were photon excesses in the target regions for SIS0 and SIS1, but the lack of distinct point sources at the optical position led us to conservatively treat these as upper limits. The sole detection in the GIS3 detector might be understood as due to the better high-energy response of the GIS detectors and the smaller off-axis angle of GIS3 compared to GIS2.

Our lower limit on the absorption column density is ≈ 20 times higher than that of GM96, and this suggests that the dust-to-gas ratio in the absorbing material may be extremely small (compare with §5.2 of GM96).

Mrk 231: This object has the lowest redshift in our sample and has sometimes been classified as a Seyfert 1, but we feel its large luminosity ($L_{\rm Bol} > 10^{46}$ erg s^{-1}) and strong absorption lines justify its inclusion (e.g. it is also included in the sample of Boroson &

Meyers 1992). Mrk 231 has recently been studied with *ASCA* by Iwasawa (1999) and Turner (1999). Our spectral analysis is consistent with the analyses in these papers and thus we do not detail it here. In Table 3 we give the column density discussed in §4.1.2 of Iwasawa (1999). However, even the fitted *ASCA* column density may be substantially smaller than the true column density to the black hole region due to possible electron scattering and partial covering effects in this extremely complicated system (see §4 for further discussion).

PG 1700+518: There were no *ASCA* sources close to the optical position for this BALQSO, and we were able to place tight upper limits on the count rate for all but the SIS1 detector. A statistical photon excess in the SIS1 target region was not from any obvious point source and thus we do not consider it a detection. A 40 ks *RXTE* observation of PG 1700+518 has also been performed with principal investigator P. Green. Given that our *ASCA* observation is $\gtrsim 15$ times more sensitive than the *RXTE* observation, we expect an *RXTE* non-detection.

LBQS 2111–4335: There was clearly no point source at the optical position of the BALQSO. However, a ninth magnitude A star (HD202042) was coincident with an X-ray source detected $2.2'$ from LBQS 2111–4335 (the A star may have a late-type binary companion that creates most of the X-ray emission). We excluded the counts from this source before calculating the count rate upper limits. Even after excluding the source from the extraction region, photon counts above the noise level were still evident in the SIS0 detector. However, we do not consider this to be a detection.

PHL 5200: The *ASCA* data for this object were first presented by Mathur et al. (1995). This BALQSO was clearly detected in all but the GIS2 detector. We find that the results of spectral analysis are highly sensitive to the details of the background subtraction. Given this sensitivity, our analyses suggest that any column density from 0–5×10^{23} cm^{-2} is consistent with the ASCA data (even at 68% confidence). Thus, while the *ASCA* data certainly do not rule out the presence of a large column density absorber, they do not convincingly show one to be present either.

4. Conclusions and Future Prospects

We have presented the first moderate-sized sample of sensitive BALQSO observations in the 2–10 keV band. This band is potentially an important one for BALQSO spectroscopy due to the ability of > 2 keV X-rays to penetrate large column densities, and the properties of our sample are likely to be more representative of the behavior of the BALQSO population as a whole than those derived from the two single-object *ASCA* studies to date (see §1). While we detect a significantly larger fraction of our objects than GM96, we find that in general even the optically brightest BALQSOs known are extremely weak in the 2–10 keV band. Assuming that our BALQSOs have typical RQ QSO X-ray continua and are weak due to intrinsic X-ray absorption, we find column densities $\gtrsim 5 \times 10^{23}$ cm^{-2} in several cases. These are the largest X-ray column densities yet inferred for BALQSOs, being about an order of magnitude larger than the lower limits of GM96. If the same outflowing gas makes both the X-ray and ultraviolet absorption, our improved column density limits also raise the implied mass outflow rate and kinetic luminosity by about an order of magnitude.

Alternatively, it is possible that BALQSOs are intrinsically X-ray weak, perhaps due to an orientation dependence of the X-ray continuum flux. Krolik & Voit (1998) have discussed the possibility of optical/ultraviolet continuum anisotropy in BALQSOs (due to accretion disk limb-darkening which dims objects viewed equatorially), but they suggest that anisotropy of the X-ray emission is likely to be weaker. If the power-law X-ray emission of RQ QSOs indeed originates in an optically thin accretion disk corona near a Kerr black hole, the intrinsic equatorial emission may in fact be enhanced by relativistic effects (e.g. Cunningham 1975).

An important corollary of our work is that optical brightness (in the B or R bands) is *not* a good predictor of X-ray brightness for BALQSOs. Two of the four BALQSO X-ray detections in our sample (0226–104 and PHL 5200) are actually among our optically faintest objects. It appears that the prototype of the class, PHL 5200 (Lynds 1967), has an unusually high X-ray flux for a BALQSO given its optical flux, and thus its X-ray properties cannot be taken as representative of the BALQSO population. In fact, its X-ray brightness is typical of non-BALQSOs of its optical magnitude, and we do not find the evidence for a large intrinsic column density in this object to be compelling (see §3). Finally, all four of our detected BALQSOs have notably high optical continuum polarizations (2.3–5%; Schmidt, Hines & Smith 1997; 7 of our 8 BALQSOs have optical continuum polarization data in the literature), and it is worth investigating if high-polarization BALQSOs tend to be the X-ray-brighter members of the class. We refrain from making a formal claim about this issue at present due to our limited sample size, but another example of this phenomenon may be IRAS 13349+2438 (see §3.1.3 of Brandt et al. 1997). High optical continuum polarization and X-ray flux could occur together if the direct lines of sight into the X-ray nuclei of BALQSOs were usually blocked by extremely thick material (say $\sim 10^{25}$ cm^{-2}). In this case, one could only hope to detect X-rays when there is a substantial amount of electron scattering in the nuclear environment by a 'mirror' of moderate Thomson depth. Then, any measured X-ray column density for a highly polarized BALQSO (e.g. Mrk 231 and PHL 5200) might not reflect the true column density to the black hole region but rather the column density along the electron-scattered path (compare with §5 of Goodrich 1997).

We have also looked for other common properties of our four X-ray detected BALQSOs and none is apparent. For example, they are not all 'PHL 5200-like' BALQSOs (see Turnshek et al. 1988).

Aside from the physical constraints placed upon the X-ray column densities in BALQSOs, our results also have important practical implications for future X-ray spectroscopy of these objects. Consider the representative case of PG 1700+518. The *ASCA* SIS and GIS count rates for this BALQSO are $< 3.2 \times 10^{-3}$ count s^{-1}, and its 2–10 keV observed flux is constrained to be $< 3 \times 10^{-13}$ erg cm^{-2} s^{-1}. Using PIMMS, this translates into an observed *AXAF* ACIS-I count rate of $< 9 \times 10^{-3}$ count s^{-1}. While this BALQSO may be detectable with *AXAF*, high-quality spectroscopy of it will be difficult and perhaps impossible (assuming no strong variability). Even in the most optimistic case, where the flux is just below our upper limit, it will take ≈ 110 ks to obtain the ≈ 1000 counts needed for moderate-quality spectroscopy.[3] A high-quality ($\approx 10\,000$ count) spectrum would require an immodest $\gtrsim 10^6$ s of *AXAF* time. For the *XMM* EPIC-PN, the count rate will be $< 2.6 \times 10^{-2}$ count s^{-1}. Spectroscopy may be more tractable in this case, but it will still prove inordinately expensive if the flux is a factor of a few times smaller than our *ASCA* upper limit. We also comment that some of our implied column density lower limits are close to becoming optically thick to Thomson scattering. If the X-ray column densities in many BALQSOs are optically thick to Thomson scattering, this will make it difficult to improve the above situation by observing at even higher energies.

5. Acknowledgments

We thank M. Elvis, E. Feigelson, E. Gotthelf, J. Krolik, A. Laor, K. Mukai, D. Schneider and an anonymous referee for helpful discussions. This paper is based upon work supported by NASA grant NAG5-4826 (SCG), the NASA LTSA program (WNB), NASA contract NAS-38252 (RMS), and NASA grants NAG5-3249 and NAG5-3390 (SM).

---

[3] The 1000 count and 10 000 count criteria are those given in §1.5 of the *AXAF Proposers' Guide*, and we find that these criteria work well in practice. Similar criteria are adopted in figures 29–33 of the *XMM Users' Handbook*.

REFERENCES

Anders, E. & Grevesse, N. 1989, Geochimica et Cosmochimica Acta, 53, 197

Arav, N. 1997, in Mass Ejection from AGN, ed. Arav, N., Shlosman, I. & Weymann, R. J. (ASP Press: San Francisco), p. 208

Arnaud, K. A. 1996, in Astronomical Data Analysis Software and Systems V: ASP Conference Series 101, ed. Jacoby, G. & Barnes, J. (ASP Press, San Francisco), p. 17

Boroson, T. A. & Meyers, K. A. 1992, ApJ, 397, 447

Brandt, W. N., Mathur, S., Reynolds, C. S. & Elvis, M. 1997, MNRAS, 292, 407

Cunningham, C. T. 1975, ApJ, 202, 788

de Kool, M. & Begelman, M. C. 1995, ApJ, 455, 448

Elvis, M., Lockman, F. J. & Wilkes, B. J. 1989, AJ, 97, 777

Giommi, P., Angelini, L. & White, N. 1997, The XIMAGE Users' Guide: Version 2.53. NASA/GSFC, Greenbelt

Goodrich, R. W. 1997, ApJ, 474, 606

Gotthelf, E. 1996, *ASCA* News, 4, 31

Green, P. J. & Mathur, S. 1996, ApJ, 462, 637 (GM96)

Hamann, F. 1998, ApJ, 500, 798

Heiles, C. & Cleary, M. N. 1979, Aust. J. Phys. Astrophys. Suppl., 47, 1

Hewett, P. C., Foltz, C. B. & Chaffee, F. H. 1995, AJ, 109, 1498

Hutchings, J. B. & Neff, S. G. 1987, AJ, 92, 14

Iwasawa, K. 1999, MNRAS, 302, 96

Kopko, M., Turnshek, D. A. & Espey, B. R. 1994, in Multi-Wavelength Continuum Emission of AGN, ed. Courvoisier, T. & Blecha, A. (Kluwer, Dordrecht), p. 450

Korista, K. T. et al. 1992, ApJ, 401, 529

Kriss, G. A. et al. 1996, ApJ, 467, 629

Krolik, J. H. & Voit, G. M. 1998, ApJ, 497, L5

Laor, A., Fiore, F., Elvis, M., Wilkes, B. J. & McDowell, J. C. 1994, ApJ, 435, 611

Laor, A., Fiore, F., Elvis, M., Wilkes, B. J. & McDowell, J. C. 1997, ApJ, 477, 93

Lawrence, A., Elvis, M., Wilkes, B. J., McHardy, I. & Brandt, W. N. 1997, MNRAS, 285, 879

Lockman, F. J. & Savage, B. D. 1995, ApJS, 107, 1

Lynds, C. R. 1967, ApJ, 147, 396

Mathur, S., Elvis, M. & Singh, K. P. 1995, ApJ, 455, L9

Marshall, H. L., Tananbaum, H., Zamorani, G. & Huchra, J. P. 1983, ApJ, 269, 42

McMahon, R. G. & Irwin, M. J. 1992, in Digitised Optical Sky Surveys, ed. MacGillivray, H. T. & Thomson, E. B. (Kluwer, Dordrecht), p. 417

Morris, S. L., Weymann, R. J., Anderson, S. F., Hewett, P. C., Foltz, C. B., Chaffee, F. H., Francis, P. J. & MacAlpine, G. M. 1991, AJ, 102, 162

Mukai, K. 1997, The PIMMS Users' Guide. NASA/GSFC, Greenbelt

Murphy, E. M., Lockman, F. J., Laor, A. & Elvis, M. 1996, ApJS, 105, 369

Nandra, K., Fabian, A. C., Brandt, W. N., Kunieda, H., Matsuoka, M., Mihara, T., Ogasaka, Y. & Terashima, Y. 1995, MNRAS, 276, 1

Neugebauer, G., Green, R. F., Matthews, K., Schmidt, M., Soifer, B. T. & Bennett, J. 1987, ApJS, 63, 615

Pier, E. A. 1997, *ASCA* Getting Started Guide for Revision 2 Data: Version 6.1. NASA/GSFC, Greenbelt

Reeves, J. N., Turner, M. J. L., Ohashi, T. & Kii, T. 1997, MNRAS, 292, 468

Schmidt, M. & Green, R. F. 1983, ApJ, 269, 352

Schmidt, G. D., Hines, D. C. & Smith, P. S. 1997, in Mass Ejection from AGN, ed. Arav, N., Shlosman, I. & Weymann, R. J. (ASP Press: San Francisco), p. 106

Sirola et al. 1998, ApJ, 495, 659

Stark, A. A., Gammie, C. F., Wilson, R. W., Bally, J., Linke, R.A., Heiles, C. & Hurwitz, M. 1992, ApJS, 79, 77

Stocke, J. T., Morris, S. L., Weymann, R. J. & Foltz, C. B. 1992, ApJ, 396, 487

Turner, T. J. 1999, ApJ, in press (astro-ph/9808090)

Turnshek, D. A., Foltz, C. B., Grillmair, C. J. & Weymann, R. J. 1988, ApJ, 325, 651

Turnshek, D. A., Monier, E. M., Sirola, C. J. & Espey, B. R. 1997 ApJ, 476, 40

Turnshek, D. A. et al. 1994, ApJ, 428, 93

Vignali, C., Comastri, A., Cappi, M., Palumbo, G. G. C., Matsuoka, M. & Kubo, H. 1999, ApJ, in press (astro-ph/9812176)

Weymann, R. J., Morris, S. L., Foltz, C. B. & Hewett, P. C. 1991, ApJ, 373, 23

Weymann, R. J. 1997, in Mass Ejection from AGN, ed. Arav, N., Shlosman, I. & Weymann, R. J. (ASP Press: San Francisco), p. 3

Wilkes, B. J., Tananbaum, H., Worrall, D. M., Avni, Y., Oey, M. S. & Flanagan, J. 1994, ApJS, 92, 53

Zamorani, G. et al. 1981, ApJ, 245, 357

Table 1. BALQSO General Information and Observing Log

Target Name[a]	z	B/R[b]	Galactic $N_{\rm H}$ /(10^{20} cm^{-2})	Obs. Date	SIS Exp. (ks)/ CCD Mode[c]	GIS Exp. (ks)[d]
PG 0043+039	0.384	15.9[(1)]/15.6[(2)]	3.0[(9)]	21 Dec 96	22.7/2 CCD	28.3
0043+008	2.146	18.4[(3)]/17.7[(4)]	2.0[(10)]	09 Jul 98	23.0/1 CCD	23.9
0226–104	2.256	17.3[(5)]/15.2[(4)]	2.6[(11)]	17 Jul 98	24.4/1 CCD	23.0
IRAS 07598+6508 (L)	0.149	14.5[(6)]/13.1[(3)]	4.5[(12)]	29 Oct 96	37.2/1 CCD	41.7
Mrk 231 (L)	0.042	14.5[(7)]/13.2[(7)]	1.0[(10)]	05 Dec 94	15.7/2 CCD	20.0
PG 1700+518 (L)	0.292	15.4[(1)]/14.4[(3)]	2.5[(9)]	24 Mar 98	19.2/1 CCD	20.6
LBQS 2111–4335	1.708	16.7[(8)]/16.0[(3)]	4.2[(13)]	23 Apr 98	21.5/1 CCD	22.6
PHL 5200	1.981	18.0[(5)]/17.4[(4)]	4.8[(11)]	21 Jun 94	10.2/2 CCD	16.4

[a]An 'L' in parentheses after the target name indicates that this BALQSO is known to show low-ionization BALs (see Boroson & Meyers 1992 and references therein). The optical spectrum for LBQS 2111–4335 presented in Morris et al. (1991) suggests that broad Al III absorption may be present. However, the current data do not allow a definitive classification (S. Morris, private communication).

[b]Magnitudes have not been corrected for BALs. The R magnitude is defined as noted in the table references.

[c]All SIS observations were done in Faint mode.

[d]All GIS observations were done in Pulse Height (PH) mode.

[1]Schmidt & Green (1983) [2]Neugebauer et al. (1991); R computed from continuum fluxes [3]McMahon & Irwin (1992)—APM catalogue; photographic E [4]Sirola et al. (1998); Gunn r [5]Stocke et al. (1992) [6]Turnshek et al. (1997) [7]Hutchings & Neff (1997); Johnson R [8]Hewett, Foltz & Chaffee (1995)

[9]Lockman & Savage (1995) [10]Elvis, Lockman & Wilkes (1989) [11]Stark et al. (1992) [12]Murphy et al. (1996) [13]Heiles & Cleary (1979)

Table 2. *ASCA* Detector Count Rates[a]/(10^{-3} photons s^{-1}).

Target Name	SIS0	SIS1	GIS2	GIS3	Observed F^{b}_{2-10}
PG 0043+039	< 1.6	< 1.6	< 1.8	< 1.9	< 2
0043+008	< 2.2	< 2.1	< 2.3	$< 4.4^{c}$	< 1
0226–104	2.5	< 2.2	2.2	5.1	1
IRAS 07598+6508	$< 2.3^{c}$	$< 3.3^{c}$	< 1.7	4.2	$\lesssim 4$
Mrk 231	7.2	6.4	6.0	7.1	8
PG 1700+518	< 1.9	$< 3.2^{c}$	< 2.3	< 2.4	< 3
LBQS 2111–4335	$< 4.0^{c}$	< 2.1	< 2.3	< 2.5	< 2
PHL 5200	3.8	6.3	< 2.9	6.3	1

[a]SIS/GIS count rates are for 0.6–9.5 keV/0.9–9.5 keV, and count rate upper limits are for 3σ unless otherwise noted.

[b]F_{2-10} is the observed 2–10 keV flux in units of 10^{-13} ergs cm^{-2} s^{-1} computed using a power law with $\Gamma = 2$. For the intrinsic column density we use either 1×10^{23} cm^{-2} or the value from column three of Table 3 (whichever is larger). The Galactic column density is also included (see §2.2).

[c]Photon excess above 3σ in the target region, but no evidence of a point source at the optical position of the target. See §3 for discussion.

Table 3. Limits on Intrinsic Absorption[a]

Target Name	Assumed X-ray Photon Index	SIS0/GIS3 Intrinsic $N_{\rm H}/(10^{22}\ {\rm cm}^{-2})$[b]
PG 0043+039	1.7	$> 47/> 40$
	2.0	$> 33/> 26$
0043+008	1.7	$> 1.8/\cdots$
	2.0	$\cdots/\cdots$
0226–104	1.7	$\cdots/\cdots$
	2.0	$\cdots/\cdots$
IRAS 07598+6508	1.7	$> 72/50$
	2.0	$> 56/36$
Mrk 231[c]	1.8	4
PG 1700+518	1.7	$> 59/> 53$
	2.0	$> 44/> 36$
LBQS 2111–4335	1.7	$> 2.6/> 3.9$
	2.0	$\cdots/\cdots$
PHL 5200	1.7	$\cdots/\cdots$
	2.0	$\cdots/\cdots$

[a]For $\alpha_{\rm ox} = 1.6$, unless otherwise noted.

[b]An ellipsis indicates that the intrinsic column density was consistent with 0 cm^{-2}.

[c]For details on the photon index and column density constraints for Mrk 231 see §3, Iwasawa (1999), and Turner (1999).

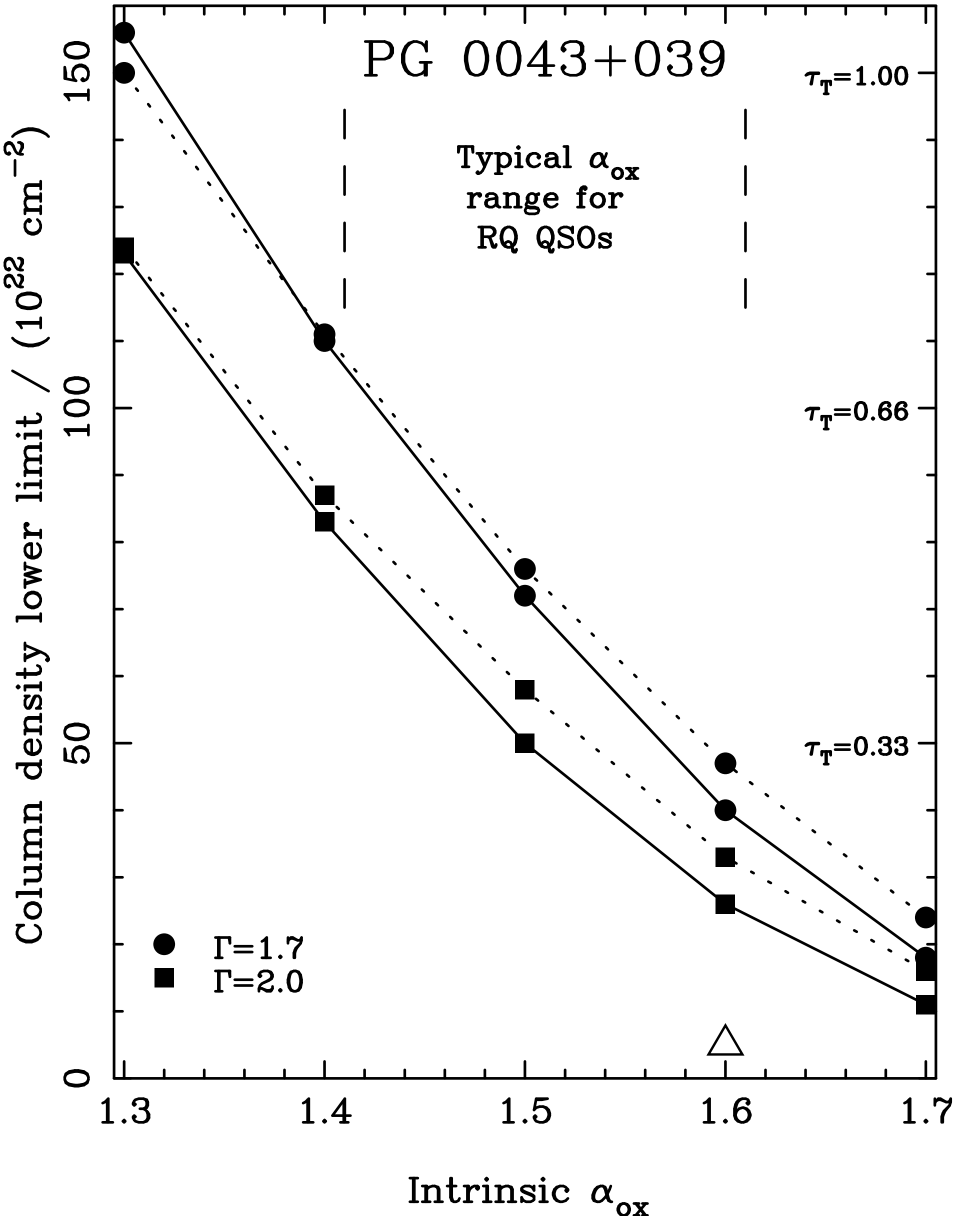

Fig. 1.— Column density lower limits for PG 0043+039 derived following the method described in the text. We show the inferred column density lower limit as a function of the intrinsic (i.e. corrected for X-ray absorption) $\alpha_{\rm ox}$. The square data points are for an X-ray photon index of $\Gamma = 2.0$ and the circular dots are for an X-ray photon index of $\Gamma = 1.7$. The dotted lines show the constraints from SIS0, and the solid lines show the constraints from GIS3. The open triangle at an intrinsic $\alpha_{\rm ox} = 1.6$ illustrates the typical BALQSO column density lower limit found by GM96 based on *ROSAT* data (although GM96 did not present *ROSAT* data for PG 0043+039). The two vertical dashed lines show the typical range of $\alpha_{\rm ox}$ for RQ QSOs (see the text). The numbers along the right hand side of the plot show the Thomson optical depth of the corresponding column density. Note that our inferred column densities are within a factor of ≈ 3 of being optically thick to Thomson scattering.

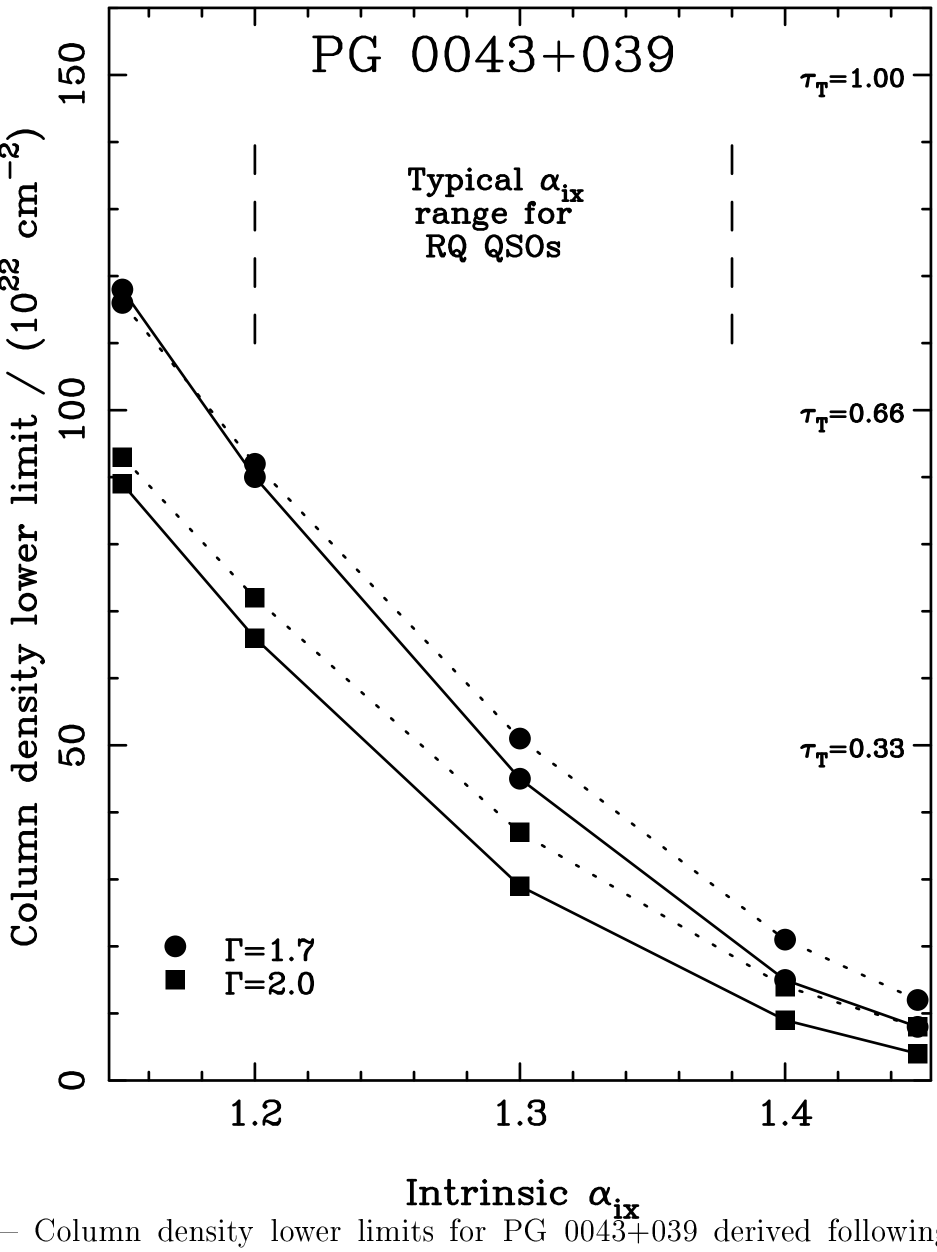

Fig. 2.— Column density lower limits for PG 0043+039 derived following the method described in the text. We show the inferred column density lower limit as a function of the intrinsic (i.e. corrected for X-ray absorption) α_{ix}. The symbols and line styles are as for Figure 1, and the typical range of α_{ix} is discussed in the text.